Rock and Soil Mechanics

Volume 43 | Issue 5 Article 8

7-4-2022

Numerical analysis of the impact of internal erosion on underground structures: application to tunnel leakage

Ying-jing LIU
Zhongtian Construction Group Co., Ltd., Hangzhou, Zhejiang 310009, China

Jie YANG
Department of Civil and Environmental Engineering, The Hong Kong Polytechnic University, Hong Kong, China

Zhen-yu YIN
Department of Civil and Environmental Engineering, The Hong Kong Polytechnic University, Hong Kong, China

Rock and Soil Mechanics 2022 43(5): 1383−1390 ISSN 1000−7598
https: //doi.org/10.16285/j.rsm.2021.6462 rocksoilmech.researchcommons.org/journal

Numerical analysis of the impact of internal erosion on underground structures: application to tunnel leakage

LIU Ying-jing[1], YANG Jie[2], YIN Zhen-yu[2]

1. Zhongtian Construction Group Co., Ltd., Hangzhou, Zhejiang 310009, China

2. Department of Civil and Environmental Engineering, The Hong Kong Polytechnic University, Hong Kong, China

Abstract: When groundwater leaks into the tunnel from damaged joints or cracks of the linings, fine particles could be pulled off from the soil matrix by seepage force and transported into the tunnel. Currently, very limited attention has been paid to the effect of the loss of fine particles induced by the water leakage, i.e. the internal erosion. In this study, the evolution of soil porosity, gradation, seepage flow, the induced ground movement and lining stress change due to tunnel leakage has been numerically investigated using a novel coupled hydromechanical approach formulated within the continuous porous medium framework. A critical state based constitutive model considering the influence of the fines content has been implemented for modelling the mechanical consequences of internal erosion. The numerical results show the spatial and temporal evolution of the eroded zone and the hydromechanical response of the tunnel and its surroundings. The results indicate that the commonly used pore pressure reduction-based method without considering internal erosion will underestimate the leakage induced lining stress change and ground movement. Moreover, the influences of three-dimensional condition are highlighted.

Keywords: tunnel; silty sand; fine particles; finite element method; internal erosion; seepage

1 Introduction

Tunnels are one of the most widely used underground structures in urban development. However, as tunnel projects gradually enter long-term service, post-construction settlements of the tunnel and surrounding soil become increasingly significant[1–2]. For example, the long-term cumulative settlement in the shield tunnel of Shanghai Metro Line 1 reached 290 mm during the 16 years of operation between 1995 and 2011. The depth and width of ground settlement in the Jubilee Tunnel Extension have continued to increase over the five years' monitoring period after the completion of construction[3]. Extensive studies have investigated the factors causing tunnel settlement, including ground deformation, groundwater changes, water seepage, and train dynamic response[4–7]. Among them, tunnel leakage is one of the key factors affecting post-construction ground and tunnel settlements[8–9].

Shield tunnels built in saturated soils may suffer from the misalignment of segment joints and segment cracks due to the combined effect of ground loads and adjacent engineering activities. As a result, leakage often occurs in areas such as segment joints, cracks, and grout holes. Previous research used the Darcy's law to analyze the effect of pore water pressure reduction on the ground and tunnel structure[10–12], and mainly focused on reducing pore water pressure and ignoring the loss of fine particles caused by leakage. However, groundwater flow caused by seepage can lead to that fine particles within the soil skeleton may be detached from the soil matrix and moving through the voids under the action of the seepage field, which is known as internal erosion[13]. The loss of fine particles can cause variations in void ratio and soil gradation, impairing soil's mechanical properties[14–16]. At the same time, void ratio change can also affect the soil permeability, which, in turn, influences the erosion process within the soil. However, research on internal erosion of soil mainly focused on dams[17–19], while the effect of erosion on tunnels has been neglected. Therefore, this paper proposese a coupled hydro-mechanical method based on the theory of porous continuous medium, which considers the internal erosion process and the effect of fine particle loss on the mechanical properties of soil. Numerical studies have been conducted to investigate the ground deformation caused by tunnel seepage in silty sand and the impact on the tunnel structure.

2 Coupled hydromechnical model

2.1 Conservation of mass and particle transport

According to Schaufler et al.[20], the saturated porous medium system is composed of four constituents: the stable fabric of the solid skeleton, the erodible fines, the fluidized particles and the pure fluid phase. The fines can behave either as a fluid-like (fluidized particles) or as a solid-like (erodible fines) material. The conservation of mass for the mixed systems[17] is given by

$$\mathrm{div}\boldsymbol{q}_{\mathrm{w}} + \mathrm{div}\boldsymbol{v}_{\mathrm{s}} = 0 \tag{1}$$

$$-\frac{\partial \phi}{\partial t} + \mathrm{div}\boldsymbol{v}_{\mathrm{s}} - \mathrm{div}\left(\phi \boldsymbol{v}_{\mathrm{s}}\right) = \hat{n} \tag{2}$$

Received: 30 August 2021 Revised: 20 January 2022
This research was supported by the Council Project (RGC) of Hong Kong Special Administrative Region Government (HKSARG) of China (15217220).
First author: LIU Ying-jing, male, born in 1985, PhD, Senior engineer, mainly engaged in research on tunnel engineering design and construction technology.
Corresponding author: YANG Jie, male, born in 1990, Postdoc, research interests: geotechnical engineering design and risk analysis, soil constitutive model and multi-field coupling analysis. E-mail：doc.jie.yang@gmail.com

$$\frac{\partial f_{\mathrm{c}}}{\partial t}-\frac{\partial\left(f_{\mathrm{c}}\phi\right)}{\partial t}+\operatorname{div}\left(f_{\mathrm{c}}\boldsymbol{v}_{\mathrm{s}}\right)-\operatorname{div}\left(f_{\mathrm{c}}\phi\boldsymbol{v}_{\mathrm{s}}\right)=\hat{n} \tag{3}$$

$$\frac{\partial\left(c\phi\right)}{\partial t}+\operatorname{div}\left(c\boldsymbol{q}_{\mathrm{w}}\right)+\frac{\partial\left(c\phi\boldsymbol{v}_{\mathrm{s}}\right)}{\partial t}=-\hat{n} \tag{4}$$

where ϕ, f_{c} and c denote the porosity, the amount of erodible fines and the concentration of the fluidized particles, respectively; t denotes the time; $\hat{n}$ represents the rate of phase transition for fine particles from solid to fluidized particles; $\boldsymbol{v}_{\mathrm{s}}$ is the first-order time derivative of the soil skeleton displacement $\boldsymbol{u}$; $\boldsymbol{q}_{\mathrm{w}}$ denotes the volume discharge rate, which is given by the Darcy's law:

$$\boldsymbol{q}_{\mathrm{w}}=-\frac{k}{\eta_k\overline{\rho}}[\operatorname{grad}p_{\mathrm{w}}-\overline{\rho}\boldsymbol{g}] \tag{5}$$

where η_k is the kinematic viscosity of the fluid; $\boldsymbol{g}$ is the gravitational field vector; p_{w} is the pore fluid pressure; k is the intrinsic permeability of the medium; and $\overline{\rho}$ is the density of the mixture. The calculation for k and $\overline{\rho}$ is given by

$$k=k_0\frac{\phi^3}{(1-\phi)^2} \tag{6}$$

$$\overline{\rho}=c\rho_{\mathrm{s}}+(1-c)\rho_{\mathrm{f}} \tag{7}$$

where ρ_{s} and ρ_{f} are the densities of the solid and fluid; and k_0 is the hydraulic conductivity of Kozeny–Carman model[21].

2.2 Erosion law

The variable $\hat{n}$ in Eqs.(2)–(4) is the volume of mass exchange, corresponding to the rate of eroded mass volume and filtrated mass volume. Different erosion laws have been proposed in recent years based on actual engineering and indoor test results[13, 22–25]. In this study, the rate of the eroded mass used is given by[22]

$$\hat{n}=-\lambda_{\mathrm{e}}f_{\mathrm{c}}\left|\boldsymbol{q}_{\mathrm{w}}\right| \tag{8}$$

where λ_{e} is a material constant. In addition, the residual fine content fraction $f_{\mathrm{c,r}}$, i.e. the maximum content of fines that can be retained within the soil skeleton at the corresponding hydraulic gradient, is introduced in the subsequent analysis.

2.3 Critical state model

In previous studies, the effect of fine particle loss on the mechanical properties of soils has often been considered by the degradation of the elastic and plastic parameters of the soil[10–12]. However, the loss of fine particles causes changes in soil's void ratio, compactness, gradation and particle contact, thus the parameter reduction method cannot directly consider the effect of particle loss on the mechanical properties of the soil. Experiments have shown that the location of the critical state line (CSL) in sand-soil mixtures is directly related to the fines content[14]. To assess the mechanical responses of the loss of the fines induced by the internal erosion, a non-associated elastoplastic constitutive model related to particle gradation is adopted to consider the influence of internal erosion on the mechanical properties of soils by incorporating the position of CSL with the fines content and compactness in e– p' plane (e is void ratio, p' is mean effective stress). This model has been extended from the basic SIMSAND model[26] (Tables 1 and 2) within the framework of the critical state concept and elastoplasticity theory which considers the effect of changes in porosity and fines content caused by erosion on the mechanical properties of soil by introducing a unified CSL formulation for mixed silt-sand soils from pure silt to pure sand[27]:

$$e_{\mathrm{c}}=e_{\mathrm{cr}0}-\lambda\left(\frac{p'}{p_{\mathrm{at}}}\right)^{\xi} \tag{9}$$

Table 1 Basic constitutive equations of SIMSAND model[26]

Type	Equation
Elastic part	$\dot{\varepsilon}_{ij}^{e}=\frac{1+\nu}{3K(1-2\nu)}\dot{\sigma}'_{ij}-\frac{\nu}{3K(1-2\nu)}\dot{\sigma}'_{kk}\delta_{ij}$ $K=K_0p_{\mathrm{at}}\frac{(2.97-e)^2}{(1+e)}\left(\frac{p'}{p_{\mathrm{at}}}\right)^n$
Shear yield surface	$f_{\mathrm{s}}=\frac{q}{p'}-H$
Plastic potential surface	$\frac{\partial g_{\mathrm{s}}}{\partial p'}=A_{\mathrm{d}}\left(M_{\mathrm{pt}}-\frac{q}{p'}\right)$ $\frac{\partial g_{\mathrm{s}}}{\partial s_{ij}}=\{1\ 1\ 1\ 1\ 1\ 1\}$
Hardening criterion	$H=\frac{M_{\mathrm{p}}\varepsilon_{\mathrm{d}}^{\mathrm{p}}}{k_{\mathrm{p}}+\varepsilon_{\mathrm{d}}^{\mathrm{p}}}$
CSL	$e_{\mathrm{c}}=e_{\mathrm{cr0}}-\lambda\left(\frac{p'}{p_{\mathrm{at}}}\right)^{\xi}$
Particle interlocking effect	$\tan\varphi_{\mathrm{p}}=\left(\frac{e_{\mathrm{c}}}{e}\right)\tan\varphi_{\mathrm{u}}\ \ \tan\varphi_{\mathrm{pt}}=\left(\frac{e}{e_{\mathrm{c}}}\right)\tan\varphi_{\mathrm{u}}$

Note: $\dot{\varepsilon}^{e}$ is the elastic strain increment; i, j, k are the coordinate components; δ_{ij} is the Kronecker symbol; $\varepsilon_{\mathrm{d}}^{\mathrm{p}}$ is the plastic deviatoric strain; $\dot{\sigma}'$ is the effective stress increment; q is the deviatoric stress; s is the deviatoric stress; p_{at} is the atmospheric pressure; K is the bulk moduli; e is the void ratio determined by the initial void ratio e_0 and volumetric strain; f_{s} is the shear yield surface; g_{s} is the yield potential; H is the hardening parameter; φ_{p} is the peak friction angle; φ_{pt} is phase-transformation friction angle; M_{p} is the peak strength ratio; M_{pt} is the phase-transformation stress ratio; and e_{c} is the critical void ratio.

Table 2 Parameters of SIMSAND model[26]

Parameter	Description
e_0	Initial void ratio
ν	Poisson's ratio
K_0	Reference volumetric modulus (dimensionless)
n	Elastic parameters (control nonlinear stiffness)
φ_{u}	Internal friction angle
e_{cr0}	Reference critical void ratio
λ	CSL parameter
ξ	CSL parameter
A_{d}	Stress-induced dilatation parameter (0.5–1.5)
k_{p}	Plastic modulus (0.0001–0.01)

where e_{cr0} is the reference critical void ratio corresponding to the void ratio at the mean effective stress $p'=0$. It determines the position of the CSL in the $e-p'$ plane; $p_{at}=101.325$ kPa is the atmospheric pressure; λ and ξ are the material constants controlling the non-linearity of the CSL. According to Yin et al.[14], to unify the mechanical behavior of a sand-silt mixture for different fines contents, e_{cr0} is a function of the evolutive fines content:

$$e_{cr0}=[e_{hc,cr0}(1-f_c)+af_c]\frac{1-\tanh[\zeta(f_c-f_{th})]}{2}+[e_{hf,cr0}\left(f_c+\frac{1-f_c}{(R_d)^m}\right)\frac{1+\tanh[\zeta(f_c-f_{th})]}{2} \tag{10}$$

where $e_{hc,cr0}$ and $e_{hf,cr0}$ are the reference critical void ratios for the pure sand and the pure silt, respectively; and a, ζ, R_d, m and f_{th} are the material constants.

Equation (10) is mathematically structured based on the hyperbolic tangent function to ensure a continuous and smooth transition domain of critical void ratio between silty sand and sandy silt.

It should be noted that, in this study, the hydromechanical coupling effect is mainly considered from two aspects: firstly, both the loss of fine particles due to internal erosion and the deformation of the soil skeleton cause changes in void ratio, leading to changes in permeability (Eq.(6)), thus affecting the pore water pressure gradient and the flow rate, which will, in turn, affect the erosion process; secondly, the loss of fine particles changes the porosity and the location of the CSL, which in turn lead to changes in the mechanical properties of the soil.

3 Secondary development of ABAQUS

The following governing equations were obtained by combining the equations of conservation of mass and momentum to formulate the initial boundary value problem (IBVP) of internal erosion:

$$\sigma_{ij,j}-w_j=0 \tag{11}$$

$$\mathrm{div}\boldsymbol{v}_s+\mathrm{div}\boldsymbol{q}_w=0 \tag{12}$$

$$-\frac{\partial\phi}{\partial t}+\mathrm{div}\boldsymbol{v}_s-\mathrm{div}(\phi\boldsymbol{v}_s)+\lambda_e f_c|\boldsymbol{q}_w|=0 \tag{13}$$

$$\frac{\partial(c\phi)}{\partial t}+\mathrm{div}(c\boldsymbol{q}_w)+\mathrm{div}(c\phi\boldsymbol{v}_s)-\lambda_e f_c|\boldsymbol{q}_w|=0 \tag{14}$$

$$\boldsymbol{q}_w+\frac{k}{\eta_k\bar{\rho}}(\mathrm{grad}p_w-\bar{\rho}\boldsymbol{g})=0 \tag{15}$$

where $\sigma_{ij,j}$ is the partial derivative of the total stress component σ_{ij} with respect to the direction j; and w_j is the body force per unit volume.

The primary unknowns in Eqs.(11)–(15) are the soil skeleton displacement $\boldsymbol{u}$, the pore pressure p_w, the porosity ϕ, the concentration of fluidized particle c and the flow rate $\boldsymbol{q}_w$. Other unknowns, such as the kinematic velocity of the soil skeletons $\boldsymbol{v}_s$, the erodible fines f_c, the density of the mixture $\bar{\rho}$ and the intrinsic permeability k can be determined explicitly by Eqs.(5)–(7).

Equations (11)–(15) define a set of nonlinear transient partial differential equations that can be solved by secondary development using the finite element program ABAQUS. ABAQUS provides a user subroutine option (UEL) that allows users to implement nonlinear finite elements with the user-defined degrees of freedom (DOFs). Figure 1 illustrates the computational flow of the ABAQUS with the call of the UEL subroutine. In general, ABAQUS/UEL solves the overall system of nonlinear equations by Newton's method:

$$\boldsymbol{A}_{\mathrm{MATRX}}\cdot\boldsymbol{d}_N=\boldsymbol{R} \tag{16}$$

where $\boldsymbol{A}_{\mathrm{MATRX}}$ is the Jacobian matrix; $\boldsymbol{R}$ is the residual nodal fluxes or forces; and $\boldsymbol{d}_N$ is the nodal vector of the DOFs.

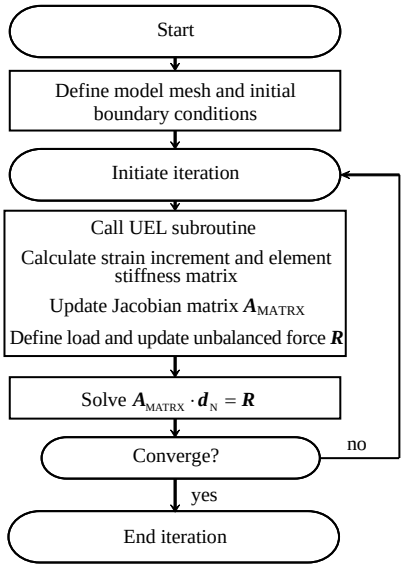

Fig. 1 Calculation flow chart in ABAQUS with call of UEL subroutine

In the UEL subroutine, the user needs to calculate strains, strain increments and nodal loads based on the displacements, displacement increments, loads and state variables passed into UEL, and update the stresses and state variables accordingly, and eventually update the Jacobian matrix ($\boldsymbol{A}_{\mathrm{MATRX}}$) and the nodal unbalance forces ($\boldsymbol{R}$). ABAQUS/UEL iteratively solves the user-defined governing equations based on $\boldsymbol{A}_{\mathrm{MATRX}}$ and $\boldsymbol{R}$ updated by the user.

Therefore, in this study, a 7-DOF ($\boldsymbol{u}(u_x,u_y)$, u_y, p_w, ϕ, c, $\boldsymbol{q}_w(q_{wx},q_{wy})$) hydromechanical coupled isoparametric plane strain erosion element and a 9-DOF ($\boldsymbol{u}(u_x,u_y,u_z)$, p_w, ϕ, c, $\boldsymbol{q}_w(q_{wx},q_{wy},q_{wz})$) hydromechanical coupled isoparametric block erosion element are developed, and the governing equations Eqs.(11)–(15) are solved by the UEL subroutine in ABAQUS. The validation of the secondary development can be found in literature[28].

4 Numerical analysis of tunnel leakage

4.1 Description of the problem

This section focuses on the impact of internal erosion caused by groundwater seepage on the tunnel and surrounding soil. The effect of the construction process of the shield tunnel on the ground is not considered in this simulation. According to Zhang et al.[29], the burial depth of shield tunnels in Shanghai is 9–15 m. A typical shield tunnel in Shanghai is shown in Fig.2, in which D is the internal diameter of the tunnel. According to Dammyr et al.[30], leakage points on the tunnel lining are usually located at the joints of segments, grouting slots and cracks in concrete pipe sheets, as shown in Fig.3. In practice, most of the leakage points are observed at the joints of the segments. Zhang et al.[29] conducted a statistical study on groundwater leakage in shield underground tunnels in Shanghai. Their findings indicated that more than 89% of the leakage points were located at the joints of the segments. Using the numerical method proposed in this paper, which considers internal erosion, this section investigates the effect of internal erosion on shield tunnels caused by tunnel leakage in the silty sand stratum.

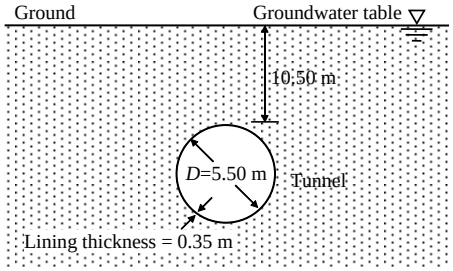

Fig. 2 Scheme of shield tunnel in numerical analysis

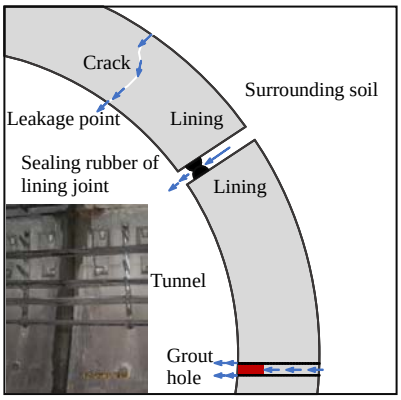

Fig. 3 Illustration of leakage points in shield tunnel and the leakage of shield tunnel in saturated soils in Shanghai

4.1.1 Numerical models

According to Yang et al.[17, 19], the three-dimensional (3D) condition is an important factor influencing the simulation results of internal erosion. Therefore, this section compares the effects of the plane strain and 3D conditions on the simulation results of internal erosion due to tunnel leakage. As shown in Fig.4, the tunnel's external diameter is 6.2 m, the inner diameter is 5.5 m, the concrete lining's thickness is 0.35 m, and the tunnel burial depth is 10.5 m. Considering the axisymmetric condition, the plane strain model uses 3456 newly developed plane strain erosion elements to model half of the analysis area; the 3D model uses 72576 newly developed brick erosion elements to model a quarter of the analysis area. The tunnel lining is modelled by a linear elastic model. The vertical boundary surface of the model is a planar symmetric boundary (roller boundary), and the bottom boundary of the model is a fully fixed boundary. The groundwater table is located at the ground, and the leakage point is located at the top of the tunnel.

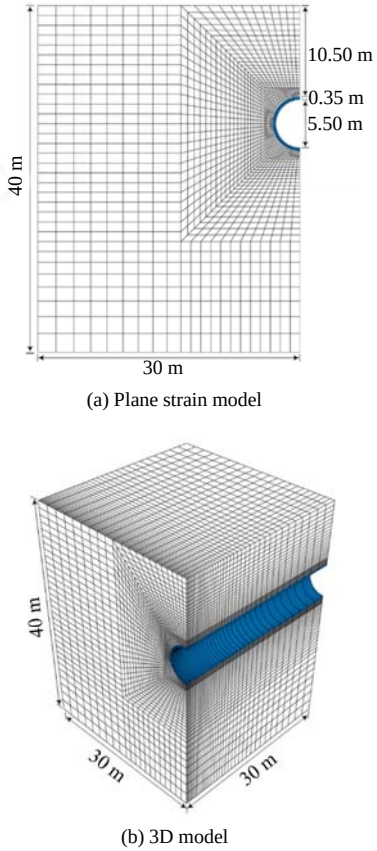

Fig. 4 Finite element mesh of numerical models

It should be noted that when the leakage point size is too large, the coarse particles of the soil skeleton will collapse into the tunnel under gravity, causing rapid disturbance to the soil around the tunnel. However, according to the field observations of groundwater seepage in shield underground tunnels in Shanghai[29], it is often only the fine particles in the soil that enter the tunnel interior with the seepage water through the leakage point. The difference in leakage point size is often reflected in the flow rate and the loss rate of fine particles from the leakage point. Therefore, in this paper, within the framework of continuum mechanics, only the loose area caused by the loss of fine particles is considered, represented by the state variables of the governing equations, without considering the cavity formed by the complete collapse of the soil. This analysis

assumes that only the point of the ground at the top of the tunnel lining is the open boundary of the leakage point, from which groundwater and fine particles can flow out by seepage and gravity.

4.1.2 Initial stress state

The initial pore water pressure and effective soil stress in the model area are initialized based on the initial groundwater table and the self-weight of the soil, where the coefficient of earth pressure at rest is $K_0 = 0.5$. After the stress initialization, the deformation of the model is reset to zero. The interaction of the lining with the soil is determined by defining the contact properties in the normal and tangential directions of the contact surfaces. In the normal direction, the contact is assumed to be rigid, allowing neither penetration nor separation; in the tangential direction, the contact is considered perfectly rough and therefore does not allow any relative slip between the two contact surfaces.

4.1.3 Model parameters

The tunnel lining is precast reinforced concrete simulated using a linear elastic constitutive model. The effect of the joint of the lining segment on the tunnel stiffness is simulated using stiffness reduction[31]. Correspondingly, the Young's modulus of the lining is 18 GPa, and the Poisson's ratio is 0.2. The soil element is simulated using a critical state model related to the fines content with material parameters corresponding to the Ottawa 50/200 sand–fine soil mixture[14], as presented in Tables 3 and 4. It should be pointed out that in this study, the model parameters are calibrated by means of optimized calibration method proposed by Yin et al.[32]. The initial void ratio of the soil is $e_0 = 0.5$, the initial fines content is $f_{c0} = 0.33$, and the initial permeability coefficient is $k_0 = 1.0 \times 10^{-8}$ m/s. Meanwhile, due to lacking of experimental data and for the sake of simplification, the residual solid fines content in this simulation is set as $f_{c,r} = 0.13$.

Table 3 Material constants of soil and fluid

Pure fluid density ρ_f /(g • cm^{-3})	Solid grain density ρ_s /(g • cm^{-3})	Kinematic viscosity of fluid η_k /(m^2 • s^{-1})
1.0	2.65	5.0×10^{-6}

Table 4 Model parameters of Ottawa sand

Elastic parameter			Plastic parameter			CSL-related parameter				Fine particle parameter			Erosion parameter
K_0 /kPa	ν	n	k_n	A_d	ϕ_d	$e_{hc\,cr0}$	$e_{fc\,cr0}$	ξ	λ	a	m	f_{th}	λ_e
130	0.25	0.52	0.0017	1	32	0.805	1.03	0.196	0.081	0	0.7	0.3	0.05

4.2 Simulation results

Figures 5 and 6 show the fines contents and ground displacement magnitude after 20 years of leakage in the two-dimensional(2D)and 3D conditions. It can be seen that the fines content around the tunnel decreases over time as internal erosion develops, forming an erosional loose zone that causes significant ground settlement above the seepage point. Compared to the plane strain simulation results, the erosion area is more concentrated near the leak point. The erosion

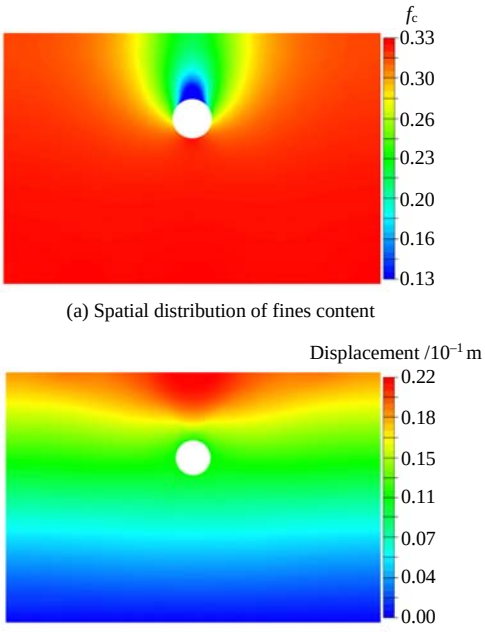

(a) Spatial distribution of fines content

(b) Displacement magnitude

Fig. 5 Spatial distribution of fines content f_c and corresponding displacement magnitude in plane strain condition during leakage

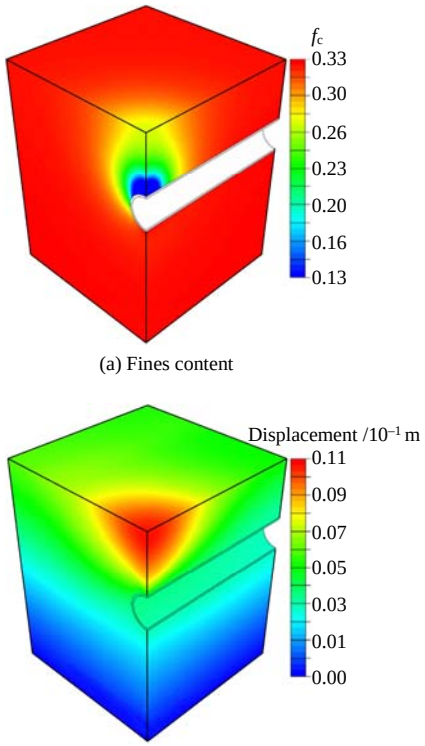

(a) Fines content

(b) Displacement magnitude

Fig. 6 Spatial distribution of fines content f_c and corresponding displacement magnitude in 3D condition during leakage

area and ground settlement develop more slowly in the 3D condition with the same parameters.

Figure 7 shows the normalized maximum ground settlement (normalized by the maximum ground settlement value after 20 years of leakage under plane strain) over time and compares the settlement caused by pore pressure reduction alone under plane strain condition (i.e. without considering the effect of internal erosion within the soil) with the settlement caused by soil erosion under plane strain and 3D conditions (i.e. considering the impact of internal erosion within the soil). The results show that when internal erosion is not considered, the reduction in pore pressure due to tunnel leakage leads to the rapid development of ground settlement at the beginning of the leakage and then to a steady-state. However, when the effect of internal erosion is considered, ground settlement due to tunnel leakage has continued to increase over the 20 years. On the one hand, as the fines content in the eroded area around the tunnel decreases, the soil's void ratio and permeability increase accordingly (Eq.(6)), leading to a continuous decrease in pore water pressure. On the other hand, the CSL moves continuously in the $e-p'$ plane as the fines content changes, reducing the strength of the eroded soil, which exacerbates the deformation of the ground. In this analysis, the settlement amount caused by the decrease in pore pressure after 20 years of seepage only accounts for 20% of the total settlement. At the same time, ground settlement in the 3D condition develops relatively more slowly than the plane strain calculation results. In the 3D condition, the soil confinement in the longitudinal direction of the tunnel limits the development of soil deformation. Moreover, in the plane strain condition, the leakage is uniformly distributed along the longitudinal direction of the tunnel, whereas in the 3D condition, it is concentrated at one point. Figure 8 shows the deviatoric plastic strain distribution in the soil around the tunnel after 20 years of leakage. It can be seen that internal erosion has caused a significant shear deformation, and induced sliding surfaces within the loosely eroded area around the leakage point, further causing subsidence of the upper soil.

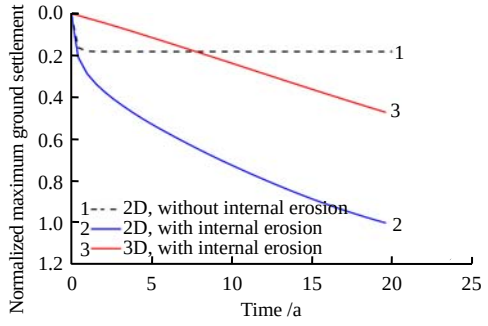

Fig. 7 Temporal evolution of the normalized maximum ground settlement

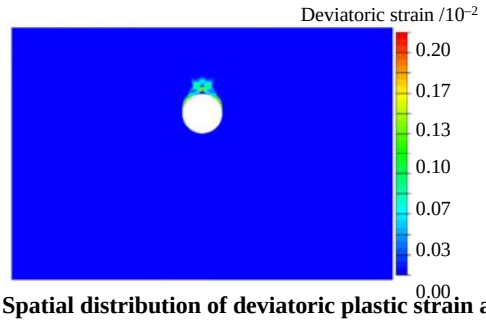

Fig. 8 Spatial distribution of deviatoric plastic strain after 20 years of leakage

Figure 9 shows the distribution of tunnel lining bending moments (normalized by the maximum tunnel lining bending moment before seepage). It can be seen that the tunnel lining bending moment increases significantly when internal erosion of soil is considered. This is due to the fact that the loss of fine particles makes the eroded soil around the tunnel looser and then redistributes the stresses around the tunnel, thus increasing the internal lining forces. Meanwhile, as the void ratio increases, the permeability of the soil increases, and the pore pressure decreases, thus increasing the soil's effective stress. In contrast, the bending moment of the tunnel lining does not change much when internal erosion of the soil is not considered. Under plane strain condition, when the internal erosion of soil is considered, the bending moments at the top, centre line and bottom of the tunnel increase by 65%, 72% and 50%, respectively, compared to the pre-leakage condition. In the 3D condition, the bending moments at the top, centre line and bottom of the tunnel increase by 35%, 41% and 27%, respectively.

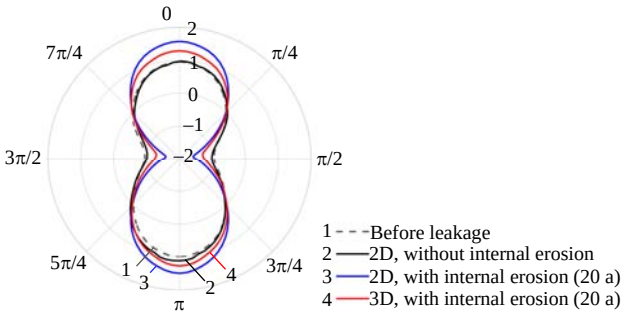

Fig. 9 Polar view of profiles of normalized bending moment of tunnel lining

Overall, approaches that only consider pore pressure reduction (e.g. Zhang et al.[29]) underestimate the change in lining stresses and the ground movement induced by tunnel leakage. In addition, the 3D condition is an important factor influencing the results of numerical calculations, including the effect on the development of eroded areas, ground settlement and the internal forces in the tunnel lining.

5 Conclusions

In this paper, a two-phase four-component model describing the internal erosion of granular materials under the action of seepage fields is developed within

the framework of continuum mechanics. A non-associated elastoplastic constitutive model related to particle gradation is adopted to consider the influence of internal erosion on the mechanical properties of soils by incorporating the position of the CSL with the fines content and compactness in $e– p'$ plane. Subsequently, the hydromechanical coupling governing equations of the internal erosion are solved through the secondary development of ABAQUS. The impact of groundwater leakage on the tunnel and surrounding soils is investigated numerically. The following main conclusions can be obtained:

(1) As internal erosion develops, the groundwater seepage creates a loose erosion zone around the tunnel, increasing the porosity and permeability of the soil near the leakage point, decreasing pore water pressure, and reducing soil strength. It ultimately leads to ground settlement above the seepage point and additional internal forces in the tunnel lining. In this analysis, tunnel seepage in three dimensions, taking into account internal erosion, increased the tunnel lining bending moment by up to 41% compared to the pre-seepage condition.

(2) The analysis based on pore pressure reduction does not consider the effect of the loss of fine particles on the permeability and mechanical properties of the eroded area. Therefore, it underestimates the changes in internal lining forces and ground movement caused by leakage. In this analysis, the amount of settlement caused by the reduction in pore pressure after 20 years of leakage is only 20% of the total settlement, while the tunnel lining bending moment does not change significantly.

(3) In addition, it was found that the 3D condition is an important factor in accurately modelling the internal erosion process: compared to the results of plane strain calculations, the constraints of the tunnel in the longitudinal direction limit the development of ground settlement in 3D conditions. At the same time, in the plane strain conditions, the leakage is uniformly distributed along the longitudinal direction of the tunnel, and the dimensions of the leakage point in that direction cannot be taken into account, thus the boundary conditions for water pressure or flow velocity at the leakage point need to be equivalently converted in the plane strain calculations.

It is important to note that the analysis in this paper aims to investigate the role of internal erosion of soil in tunnel leakage and provide a new approach to more accurately estimate the impact of seepage on tunnels. This paper provides only a qualitative analysis of the case. In practice, well-documented indoor tests or physical model tests are required to calibrate the model parameters and erosion law for more accurate quantitative analysis.

References

[1] SHEN S L, WU H N, CUI Y J, et al. Long-term settlement behaviour of metro tunnels in the soft deposits of Shanghai[J]. Tunnelling and Underground Space Technology, 2014, 40: 309–323.

[2] ZHU Qi-yin, YE Guan-lin, WANG Jian-hua, et al. Long-term settlement and construction disturbance during shield tunnelling in soft ground[J]. Chinese Journal of Geotechnical Engineering, 2010, 32(Suppl.2): 509–512.

[3] O'REILLY M, NEW B. Settlements above tunnels in the United Kingdom-their magnitude and prediction[C]//The third International Symposium. [S. l.]: [s. n.], 1982.

[4] WU H N, SHEN S L, LIAO S M, et al. Longitudinal structural modelling of shield tunnels considering shearing dislocation between segmental rings[J]. Tunnelling and Underground Space Technology, 2015, 50: 317–323.

[5] YANG Bing-ming, LIU Bao-guo. Analysis of long-term settlement of shield tunnel in soft aoil area under cyclic loading of subway train[J]. China Railway Science, 2016, 37(3): 61–67.

[6] ZHANG Dong-mei, GAO Cheng-peng, YIN Zhen-yu, et al. Particle flow simulation of seepage erosion around shield tunnel[J]. Rock and Soil Mechanics, 2017, 38(Suppl.1): 429–438.

[7] ZHANG Dong-mei, RAN Long-zhou, YAN Jing-ya, et al. Effect of grouting on tunnel leakage-induced pore pressure change in saturated soft soils[J]. Rock and Soil Mechanics, 2017, 38(12): 3427–3435.

[8] ZHANG D, HUANG Z, YIN Z, et al. Predicting the grouting effect on leakage-induced tunnels and ground response in saturated soils[J]. Tunnelling and Underground Space Technology, 2017, 65: 76–90.

[9] LIU Yin, ZHANG Dong-mei, HUANG Hong-wei. Influence of long-term partial drainage of shield tunnel on tunnel deformation and surface settlement[J]. Rock and Soil Mechanics, 2013, 34(1): 290–298.

[10] HUANGFU M, WANG M S, TAN Z S, et al. Analytical solutions for steady seepage into an underwater circular tunnel[J]. Tunnelling and Underground Space Technology, 2010, 25(4): 391–6.

[11] PARK K H, OWATSIRIWONG A, LEE J G. Analytical solution for steady-state groundwater inflow into a drained circular tunnel in a semi-infinite aquifer: a revisit[J]. Tunnelling and Underground Space Technology, 2008, 23(2): 206–9.

[12] ZHANG D M, MA L X, HUANG H W, et al. Predicting leakage-induced settlement of shield tunnels in saturated clay[J]. Computer Modeling in Engineering and Sciences, 2012, 89(3): 163–188.

[13] BONELLI S, MAROT D. Micromechanical modeling of internal erosion[J]. European Journal of Environmental and Civil Engineering, 2011, 15(8): 1207–1224.

[14] YIN Z Y, HUANG H W, HICHER P Y. Elastoplastic modeling of sand-silt mixtures[J]. Soils and Foundations, 2016, 56(3): 520–532.

[15] YANG J, YIN Z Y, LAOUAFA F, et al. Hydro-mechanical modeling of granular soils considering internal erosion[J].

Canada Geotechical Journal, 2020, 57(2): 157–172.

[16] YANG J, YIN Z Y, LAOUAFA F, et al. Analysis of suffusion in cohesionless soils with randomly distributed porosity and fines content[J]. Computers and Geotechnics, 2019, 111: 157–171.

[17] YANG J, YIN Z Y, LAOUAFA F, et al. Internal erosion in dike-on-foundation modeled by a coupled hydromechanical approach[J]. International Journal for Numerical and Analytical Methods in Geomechanics, 2019, 43(3): 663–683.

[18] ZHANG L M, CHEN QUN. Seepage failure mechanism of the gouhou rockfill dam during reservoir water infiltration[J]. Soils and Foundations, 2006, 46(5): 557–568.

[19] YANG J, YIN Z Y, LAOUAFA F, et al. Three-dimensional hydromechanical modeling of internal erosion in dike-on-foundation[J]. International Journal for Numerical and Analytical Methods in Geomechanics, 2020, 44(8): 1200–1218.

[20] SCHAUFLER A, BECKER C, STEEB H. Infiltration processes in cohesionless soils[J]. Journal of Applied Mathematics and Mechanics, 2013, 93(2-3): 138–146.

[21] REVIL A, CATHLES L. Permeability of shaly sands[J]. Water Resources Research, 1999, 35(3): 651–662.

[22] UZUOKA R, ICHIYAMA T, MORI T, et al. Hydro-mechanical analysis of internal erosion with mass exchange between solid and water[C]//6th International Conference on Scour and Erosion. Paris: [s. n.], 2012: 655–662.

[23] YANG J, YIN Z Y, LAOUAFA F, et al. Modeling coupled erosion and filtration of fine particles in granular media[J]. Acta Geotechnica, 2019, 14(6): 1615–1627.

[24] VARDOULAKIS I, STAVROPOULOU M, PAPANASTASIOU P. Hydro-mechanical aspects of the sand production problem[J]. Transport in Porous Media, 1996, 22(2): 225–244.

[25] LUO Yu-long, SU Bao-yu, SHENG Jin-chang, et al. New understandings on piping mechanism[J]. Chinese Journal of Geotechnical Engineering, 2011, 33(12): 1895–1902.

[26] JIN Y F, YIN Z Y, SHEN S L, et al. Selection of sand models and identification of parameters using an enhanced genetic algorithm[J]. International Journal for Numerical and Analytical Methods in Geomechanics, 2016, 40(8): 1219–1240.

[27] LI X S, WANG Y. Linear representation of steady-state line for sand[J]. Journal of Geotechnical and Geoenvironmental Engineering, 1998, 124(12): 1215–1217.

[28] YANG J. Numerical analyses of the multi-physics problem of sinkholes in the vicinity of a dike or a linear geo-structure[D]. Nantes: Centrale Nantes, 2019.

[29] ZHANG D M, MA L X, ZHANG J, et al. Ground and tunnel responses induced by partial leakage in saturated clay with anisotropic permeability[J]. Engineering Geology, 2015, 189: 104–115.

[30] DAMMYR Ø, NILSEN B, THURO K, et al. Possible concepts for waterproofing of norwegian TBM railway tunnels[J]. Rock Mechanics and Rock Engineering, 2014, 47(3): 985–1002.

[31] LEE K M, GE X W. The equivalence of a jointed shield-driven tunnel lining to a continuous ring structure[J]. Canada Geotechanical Journal, 2001, 38(3): 461–483.

[32] YIN Z Y, JIN Y F, SHEN S L, et al. An efficient optimization method for identifying parameters of soft structured clay by an enhanced genetic algorithm and elastic-viscoplastic model[J]. Acta Geotechnica, 2017, 12(4): 849–867.